Understanding the effect of coating drying operating variables on electrode physical and electrochemical properties of lithium-ion batteries

Román-Ramírez L.A.[a,b,]*, Apachitei G.[a,b], Faraji-Niri M.[a,b], Lain M.[a,b], Widanage W. D.[a,b] and Marco J.[a,b]

[a] Warwick Manufacturing Group, University of Warwick, CV4 7AL Coventry, United Kingdom. [b] The Faraday Institution, Quad One, Harwell Science and Innovation Campus, Didcot, UK.
*Corresponding author. E-mail: Luis.Roman-Ramirez@warwick.ac.uk.

Abstract

The effect of coating and drying process variables (comma bar gap, web speed, coating ratio, drying temperature and drying air speed) on NMC622 cathode physical properties (thickness, mass loading and porosity) and electrochemical properties (gravimetric capacity, volumetric capacity and rate performance) is studied by a design of experiments approach. Electrochemical performance is assessed on half coin cells at C-rates from C/20 up to 10C. The statistical analysis of the data reveals that the cathode physical properties are mainly affected by comma bar gap and coating ratio. The electrochemical properties also show high correlations between comma bar gap and coating ratio for some C-rates. As a second evaluation, the relationship between the cathode half-cell physical characteristics with the electrochemical performance is studied through multiple linear regression analysis. A correlation mainly between coating weight and the electrochemical properties is found. Empirical linear models representing the relationship between the output and input variables are provided, showing correlation coefficients (R^2) as high as 0.99.

Keywords

Coating, Drying, Lithium-ion batteries, Cathode, Manufacturing, Design of Experiments

1 Introduction

Driven by consumer awareness and government legislation towards zero greenhouse emissions, the global sales for battery electric vehicles (EV) is estimated to reach 31.1 million units by 2030 [1]. In the UK, for instance, the Green Industrial Revolution plan prohibits the sales of new petrol and diesel cars from 2030 [2]. The sustainable growth of EVs undoubtedly will be accompanied by an increase in research and development (R&D) on lithium-ion batteries (LiBs). Although the development of new materials, formulations and technologies are the focus of considerable research on LiBs [3-12], research on the effect of the different electrode manufacturing steps on final LiBs' performance, particularly through the understanding of operating parameters, is limited, despite also playing an important role for their continual development, increasing manufacturing efficiency and in lowering production costs [13-16].

Electrode manufacturing comprises a series of steps (mixing, coating, drying, calendering, cutting and final drying) each consisting of several process variables (operating parameters, process state variables and input material properties) and intermediate products with their own output structural features (Figure 1). Each stage contributes to the final electrode structure and resulting electrochemical performance [17-19]. It has been estimated that hundreds of process variables and intermediate product features are involved in the LiB manufacturing [17, 19-22], hindering the understanding of the contribution of each of the manufacturing stages to the final cell. Some attempts can be found in the literature to identify the contribution of process steps on electrode properties. Bockholt et al. [23] for instance, studied the relationship between process steps (mixing, coating, drying and calendering) and

electrochemical properties of NMC111 pouch cells; the influence of each process was determined based on changes in the electrode structure at every process output. Lenze et al. [24] investigated at the pilot plant scale the influence of active material mass loading, carbon black mass fraction and the degree of calendering on capacity at different C-rates. Drying temperature on binder distribution was researched by Müller et al. [25] and Jaiser et al. [26] on graphite anodes, revealing that low drying rates improve battery rate capability and cell capacity. Saraka et al. [27] studied the effect of coating and drying through analysing shear rate and drying temperature of NMC111 electrodes at laboratory scale. Other works have focused on understanding the effects of mixing sequence or mixing intensity on intermediate product properties or final electrochemical performance [28-30].

Nevertheless, studies on the effect of operating parameters (machine settings) and process state variables (e.g. drying temperature) on battery performance are rare [15], particularly at the pilot plant and industrial scale [31]. A few exceptions are the works of Bockholt et al. [32] on mixing time and mixing intensity at pilot plant scale demonstrating the influence of these parameters on electrode structure. Westphal et al. [5] studied the effect of drying parameters (temperature and air speed) on adhesion strength and resistance, for artificial graphite anodes at pilot-plant scale, concluding that optimum drying conditions exist for each mass loading and each formulation. Similarly, Westphal and Kwade [33] studied drying temperature effects on conductive additive and binder segregation, revealing that segregation increases with drying temperature.

Besides experimentation, other approaches have been used to understand the causality between the electrode performance and the process variables, and include theoretical

analysis [34], production systems simulation [15, 35, 36], uncertainty quantification [37], and machine learning [21, 38]. Schmidt et al. [15], for instance, modelled the effect of manufacturing uncertainties in the coating, drying and calendering processes on cell electrochemical properties; the analysis revealed that the highest impact on volumetric energy density is attributable to the coating process. Schönemann et al. [35] simulated the effect of four different slurry mixing routes on mixing time, viscosity density and electrode resistance. Applying machine learning techniques (Generalized Linear Model, Artificial Neural Networks, Support Vector Regression, Decision Trees, Random Forest, and Gradient Boosted Trees), Schnell et al. [21] determined a strong influence of the manufacturing steps on cell capacity, but unfortunately, details about specific parameters were not given.

In the above approaches, experimental data is still needed for model development and validation which can be difficult to acquire, particularly at large scales [35]. In this sense, experimental design or design of experiments (DoE) is a valuable tool to obtain the maximum amount of information from the minimum number of experiments [20, 39-41]. DoE is widely used in industry as part of the Failure Mode Effects Analysis (FMEA) and the Quality by Design (QbD) concept for the identification and classification of influencing parameters; the latter mainly used in the pharmaceutical industry [42, 43]. In the field of LiBs Westermeier et al. [17], Westermeier et al. [22] presented an overview of how DoE can be applied in the FMEA together with multiple domain matrices (MDM) to find the influencing parameters on the quality characteristics of the final product. Similarly, Schnell and Reinhart [44] presented a quality gate concept for the identification and management of fluctuations of intermediate products in the LiBs manufacturing process that involves DoE analysis.

In the present paper, the DoE methodology is employed for the first time to the pilot scale manufacturing of NMC622 cathodes to determine the main influencing process variables of the coating-drying step. Physical properties (thickness, mass loading, porosity) and electrochemical properties (gravimetric capacity, volumetric capacity and rate performance) are studied as a function of coating and drying operating parameters and process state variables (comma bar gap, web speed, coating ratio, drying temperature and air speed) of a comma bar coater. Correlations between the electrode properties and process variables are obtained through multiple linear regression analysis. The analysis is also used to determine the relationship between half coin cell physical characteristics and their electrochemical performance.

2 Experimental Approach

2.1 Electrode coating and drying overview

The experiments were performed on a pilot scale continuous convective coater (Megtec Systems). The equipment comprises a comma bar configuration, including a slurry reservoir with level control and a fluid delivery pump. The gap between the comma bar and the precision chrome roll controls the amount of slurry to be transferred to the chrome roll. Coating at this scale is a roll-to-roll process, the current collector is webbed and guided through the coating and dryer stages. The deposition of the slurry from the chrome roll occurs where the foil is supported by the bump roll and the two electrode components get in contact. The amount of material deposited depends on the relative speeds of the rolls through the coating ratio, which is defined as the chrome backing roll speed/bump roll speed. Machine

operating conditions for the comma bar gap, coating ratio and web speed span from 0 – 200 µm, 100 – 150% and 0 – 5 m/min, respectively.

The coater consists of three drying zones of equal length with a total of approximately 3.4 m effective drying length. Each zone has an upper and a lower drying nozzle, for which the air supply temperature and air speed values can be set in the ranges from room temperature to 180 °C and 0 – 20 m/s, respectively.

Two weight/thickness gauges (MeSys GmbH) scan across the electrode, in a zig-zag recording pattern, before and after drying, which provide the measurements for mass loading wet and mass loading dry. The system uses ultrasound to locally oscillate the electrode and provide information on the mass loading in real time.

2.2 Experimental design

The Plackett-Burman (PB) experimental design was used to identify the main factors (independent variables) of the cathode coating-drying process. PB designs are two-level fractional factorial saturated designs used for screening (study main effects) when parameter interactions are neglected [45, 46]. From an initial list of several potential factors, a final number of five factors were chosen to be included in the experimental design. This decision was based on previous experience with the process, input from expert users and studies from literature [17, 20, 22, 47]. The selected factors were comma bar gap, coating ratio, web speed, drying temperature and drying air speed. A low and a high setting were studied for each factor (Table 1), as commonly used in screening studies.

The drying temperature was only varied on the first zone based on observations that this condition is the most influential of the three drying stages. The remaining two zones were kept constant. For the case of air speed, the three zones were simultaneously varied according to the experimental design values. The experimental design was obtained in Design-Expert [48]. The final experimental matrix is shown in Table 1.

The electrode formulation and the mixing protocol (see sections 2.3 and 2.4) were kept constant throughout the experiments.

The responses (dependent variables) were measured at three different stages after the coating-drying step as presented in the parameters-diagram in Figure 2:

i) pre-calendered responses, i.e. measurements performed on the coated foils before being subjected to calendering. The responses included the coating thickness, mass loading wet, mass loading dry, porosity, spatial autocorrelation and join counting (SAJC) Z-score for carbon and for fluorine.

ii) pre-cell responses, i.e., measurements carried out on the electrode strips produced after final drying, calendering and cutting of the initial coated foils. The measurements included the calendered thickness and calendered porosity. iii) half-coin cell responses, i.e., measurements performed on the coin cells produced from the strips. The responses included the cell thickness, coating weight, cell porosity, gravimetric and volumetric capacities at different C-rates (C/20, C/5, C/2, 1C, 2C, 5C, 10C) and rate performance at 5C:C/5. Details of the physical and electrochemical characterisations are given in sections 2.5 and 2.6.

Identification of the main factors influencing each of the responses was done by statistical analysis in Design-Expert [48]. The analysis involved the analysis of variance (ANOVA) with the confidence level set to 90% (α=0.1), and graphical response for: normal plot of residuals (to check for normal distribution), predicted vs actual (to identify potential outliers) and residual vs run (to rule out the presence of time trends). The main effects model considers only the linear relationship between factors (x_i for $i = 1, 2, .. k$ number of factors) and the response (y) according to Eq. (1). In Eq. (1), ε is the random error and β_0 and β_i are regression coefficients estimated by fitting of the experimental data by the least-squares method. Significant terms (main factors) in Eq. (1) were obtained from ANOVA by forward selection based on their probability values (p-value < 0.1). A variance-stabilizing transformation to the data was applied to the cases exhibiting a non-normal distribution by modifying Eq. (1) according to $y' = y^{\lambda}$; where λ is a real number [49]. From ANOVA, the coefficient of determination (R^2) and predicted R^2 ($R_{pred}{}^2$) were obtained to determine the correlation and predictive capabilities of the model.

Table 1. Factors, levels and set of experiments (design matrix) according to the Plackett-Burman experimental design.

Factors	No. of levels	Low	High
Comma bar gap (□m)	2	80	140
Web speed (m/min)	2	0.5	1.5
Temperature[a] (°C)	2	85	110
Air speed (m/s)	2	5	15
Coating ratio (%)	2	110	150

	Design Matrix				
Experiment	Comma bar gap (□m)	Web speed (m/min)	Temperature (°C)	Air speed (m/s)	Coating ratio (%)
1	140	0.5	85	5	150
2	80	0.5	85	15	150
3	80	1.5	110	5	150
4	140	0.5	110	5	110
5	80	1.5	85	5	110
6	80	1.5	110	15	110
7	140	1.5	110	5	150
8	140	1.5	85	15	110
9	140	1.5	85	15	150
10	140	0.5	110	15	110
11	80	0.5	85	5 15	110
12	80	0.5	110		150

[a] Temperature of the first drying zone, the other two zones were held constant at 110 and 95 °C, respectively.

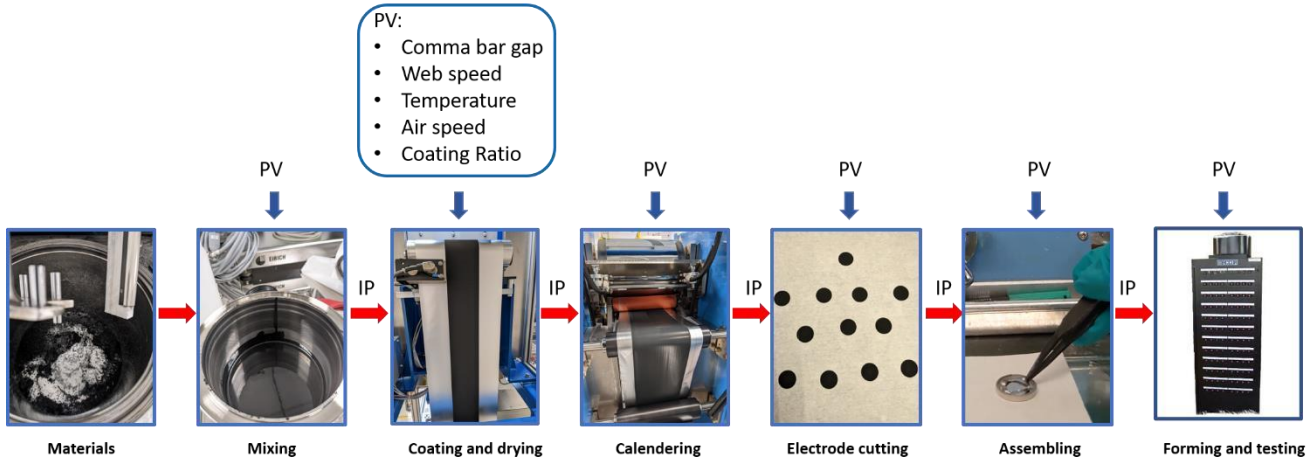

Figure 1. Schematic diagram of the electrode manufacturing process.

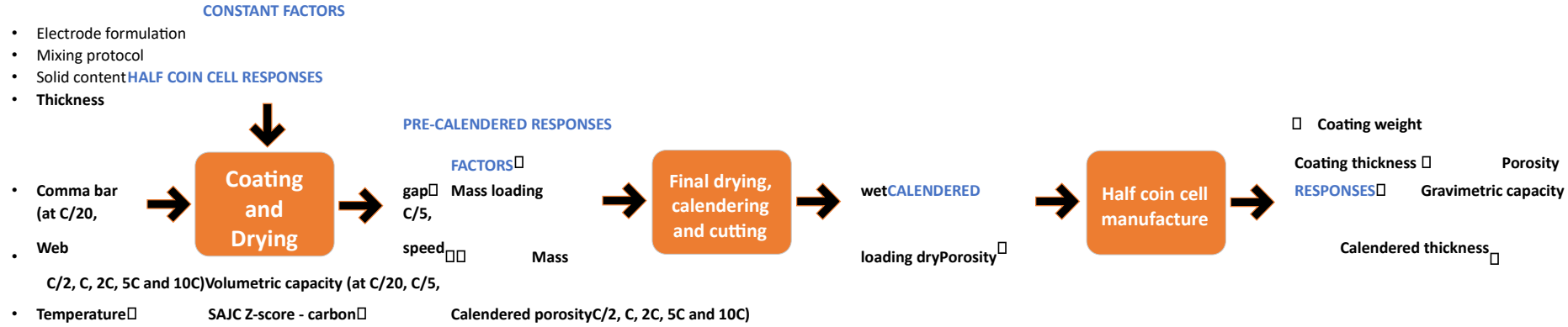

- **Air speed**
- **Coating ratio** **SAJC Z-score - fluorine** **Rate performance at 5C:C/5**

Figure 2. Parameters diagram for the coating-drying process.

$$y = \beta_0 + \sum_{i=1}^{k} \beta_i x_i + \varepsilon \quad (1)$$

2.3 Materials

The cathode material employed in the experiments consists of 96 wt% $LiNi_{0.6}Mn_{0.2}Co_{0.2}O_2$ (NMC622, BASF) active material (AM), 2 wt% C65 (Imerys) conductive additive and 2 wt% polyvinylidene difluoride (PVDF 5130, Solvay) as binder. 1-methyl-2-pyrrolidinone (NMP, ACROS Organics) was used as solvent.

2.4 Electrode and cell manufacture

2.4.1 Mixing

The electrode manufacturing process started with the dry mixing of the solid components, followed by a kneading stage in a 1 L intensive mixer (EL1, Eirich). A fraction of the solvent was added and the materials were continuously mixed until a homogeneous slurry was obtained. The rest of the solvent was then added and mixed in the dilution stage until a final slurry solid content of 67% was reached. The slurry was degassed before the coating process to remove any gas voids and prevent coating defects. The rotor speed was set to 15 m/s during dry mixing and to 10 m/s during the kneading and dilution stages, while the mixing pan speed was kept constant at 0.7 m/s.

2.4.2 Coating and drying

The slurry was coated over a 15 µm thickness aluminium current collector with the comma bar gap, coating ratio and web speeds varied according to Table 1 (experiments 1-12). The electrode was then dried in the convective oven as described in section 2.1 with the operating settings in Table 1. As highlighted, the drying temperature was only varied on the first zone, zones 2 and 3 were kept constant at 110 °C and 95 °C, respectively. The electrodes were cut into strips and calendered.

2.4.3 Calendering and cutting

To ensure a complete removal of the solvent and any possible moisture absorbed from the environment after the coating-drying process, the electrodes were further dried in a vacuum oven at 120 °C for 12 h. This procedure emulates the large-scale final drying step taking place before cell production [14]. The electrodes were then calendered using a small R&D calender (Innovative Machine Corporation) at a line speed of 0.5 m/s with the rolls heated at 85 °C. Although a porosity of 30% was targeted, since the calendering was performed on sheets of 9 cm × 15 cm using the average value of the thickness and coating weight with the target porosity at the local level where the coin cell electrodes were cut, the final porosities resulted in values ranging from 29.87% to 39.62%. Electrode discs of 14.8 mm diameter were then punched using EL-Cell electrode cutters.

2.4.4 Half-coin cell assembly

2032-type half-coin cells were manufactured with single-sided coated electrode discs having

14.8 mm diameter and a lithium foil counter electrode. Coin cell assembly was performed inside a glove box, in argon atmosphere with O_2 and H_2O levels less than 0.5 ppm. A microporous trilayer membrane (polypropylene/polyethylene/polypropylene- H1609 from
Celgard) was used as the separator. The cells were filled with 60 µl of RD281 electrolyte (1 M $LiPF_6$ in ethylene carbonate: ethyl methyl carbonate (EC:EMC) = 3:7 (v/v) + 1wt% vinylene carbonate (VC), SoulBrain). The coin cell stack included a wave spring and 1 mm thick stainless-steel spacers to achieve adequate pressure and sealing.

2.5 Physical characterisations

2.5.1 Slurry

A rotational rheometer (Anton Paar) was used to measure viscosity vs. shear rate. The solid content of the slurry was measured using a moisture analyser (Ohaus, MB120). Solid content, coating shear rate and viscosity at coating shear rate data for each of the experimental runs are presented in the Data in Brief accompanying paper [50]. To prevent defects during coatings due to large particles or clusters present in the slurry, quality checks were done using a Hegman (fineness of grind) gauge (see Data in Brief [50]).

2.5.2 Electrode

The thickness of the electrodes was measured before and after calendering by a digital thickness gauge (Mitutoyo) with a precision of 1 µm. The reported coating thickness values represent the mean from 10 different locations on a 9 cm × 15 cm electrode strip. Prior to assembly, the thickness and mass of each electrode disc used in the coin cells were measured

using the same approach. The mean values of the corresponding measurements for each electrode strip and for each of the coin cells can be found in the accompanying paper [50].

The mass loadings of the wet and dry coatings were obtained by the MeSys Systems. The recorded data (available in [50]) was further processed in MATLAB [51]. In the first step, the data was processed to remove outliers (defined as data points at least three times of the scaled median absolute deviations away from the median of the same experiment); missing recording data points (because of inevitable machine recording issues) were then replaced with the mean values of the nearest neighbour data; next, the data points were unified in terms of time resolution. In the second step, feature extraction was performed where the mean, standard deviation and median of data were calculated. A graphical example of the initial and post processed data for mass loading dry is shown in Figure S1.

The porosities (pre-calendered, calendered and cell) were calculated from the measured thickness values according to Eq. (2), where P (%) is the porosity, $\rho_{coating}$ (g/cm^3) is the effective density of the coating and ρ_{bulk} (g/cm^3) is the approximation of the coating density at 0% porosity. The coating mass loading, m (g/m^2), and thickness, $t_{coating}$ (µm), can be used to define the coating density. The values of $\rho_{coating}$ and ρ_{bulk} for each fabricated coin cell can be found in the Data in Brief article [50].

$$P = 1 - \frac{\rho_{coating}}{\rho_{bulk}} = 1 - \frac{m}{t_{coating} \cdot \rho_{bulk}} \quad (2)$$

To look for effects of operating conditions on the dispersion of conductive carbon and PVDF binder concentration at the surface of the coating, the distribution of carbon (present in both, PVDF and conductive additive) and fluorine, was determined by SAJC. Quantification of spatial autocorrelation typically uses techniques like Moran's I Index [52] and Geary's G ratio [53].

Join counting is a special example of spatial autocorrelation analysis, often employed for regular grid areas with a binary 0 or 1 parameter allocation [54]. Small disks of the cathode coatings were microtomed to give a clean edge, and then mounted on metal strips using conductive carbon tape. These samples were then examined using a desktop scanning electron microscope (SEM, Hitachi TM3030), fitted with a 30 mm^2 energy dispersive X-ray spectroscopy (EDS) detector (Oxford Instruments). The EDS maps for carbon and fluorine were converted from colour to black and white, with maximum contrast. The *.jpg files were then converted to *.txt files using ImageJ software [55]. These files were imported into an Excel spreadsheet for the join counting process. If each pixel is either 0 or 1, then the number of 1-1 joins is given by $0.5 \sum_i \sum_j z_i z_j$, where z_i and z_j are the values for box i and j, either 0 or 1, and a Z-score is calculated from $Z = (observed - expected) \,/\, standard\ deviation$. The expected and standard deviation values are calculated for a random distribution of pixels, with the same surface coverage. The EDS maps and corresponding black and white images can be found in the accompanying publication [50].

2.6 Electrochemical characterisations

The characterisations involved obtaining discharge C-rate capacities on three coin cells produced from the same coating (experiment) to capture cell-to-cell variation. The reported values of the tests are the average and the standard deviations computed from the three coin

cell measurements. The electrochemical tests were performed in a temperature-controlled chamber at 25 °C using a Maccor 4000 series battery cycler with maximum channel charge current of 5 A. The testing protocol was created with upper and lower cut-off voltages of 4.2 V and 2.5 V, respectively. Formation cycle was performed at C/20 rate, followed by five conditioning cycles at C/5. Discharge C-rate capacities were measured at C/20, C/5, C/2, 1C, 2C, 5C and 10C with all charging cycles done at C/5. C-rate capacities for each of the manufactured coin cells can be found in the Data in Brief paper [50].

The gravimetric capacity (mAh/g) was calculated by reporting the cell capacity to the active material mass (Eq (3)). The volumetric capacity (mAh/cm^3) was calculated using the electrode volume (Eq. (4)).

$$Gravimetric\ capacity = \frac{capacity}{(electrode\ mass - foil\ mass)(active\ material\ wt\%)} \quad (3)$$

$$Volumetric\ capacity = \frac{capacity}{cell\ area\ (total\ thickness - foil\ thickness)} \quad (4)$$

3 Results and Discussion

A total of 26 responses were measured for each of the 12 experimental runs. The values of the measured responses and their standard deviations are reported in the Data in Brief paper [50]. The analysis of the responses was divided into two parts. In the first part (section 3.1),

the main process variables influencing each of the responses were identified through the ANOVA for a main effects model (linear model). In the second part (section 3.2), ANOVA is employed to determine whether a relationship exists between the electrochemical performance of the half coin cells and their physical characteristics, and to obtain the relevant model. In both cases, factors with a p-value lower than 0.1 were considered statistically significant and were included in the final models. An example of the output from ANOVA and graphical response can be found in Table S1 and Figures S2-S4.

3.1 Process variables as factors

3.1.1 Effect on physical properties

The main influencing factors for the thicknesses (pre-calendered, calendered and coin cell), mass loadings (wet and dry) and cell coating weight are comma bar gap and coating ratio (Figure S6). R^2 as high as 0.99 (Figure 3) were obtained showing the strong correlation between factors and responses. The $R_{pred}{}^2$ were also considerably high ($R_{pred}{}^2$ > 0.97, Figure 3a), revealing that the models can be used for prediction purposes.

It is not surprising that comma bar gap and coating ratio are the main factors influencing thickness, mass loading and cell coating weight since there is an obvious relationship between the amount of material deposited (given by the settings of the process variables) and these properties. Nevertheless, the importance of the experimental design approach is also the capacity to obtain a mathematical model to express such relationship. The obtained models are discussed at the end of this section.

Conversely the influence of the process variables on the porosities (pre-calendered, calendered and cell) and the carbon and fluorine distributions cannot be so simply deduced. The pre-calendered porosity was explained in this case by variations in the comma bar gap, coating ratio and web speed only (Figure S5); i.e., drying temperature and air speed did not show an effect on this property. Changes in the calendered porosity and cell porosity, in contrast, could not be explained by any of the studied process variables (Figure 3a and Figure S5), meaning that other factors become more important in explaining such changes. Factors involved in the calendering step are the most evident reason (e.g. calendered pressure and roll temperature) consistent with comparable studies that examine LiB manufacturing [56].

Carbon and fluorine distributions (as determined by SAJC Z-score) also did not show a statistically significant relationship with the operating variables. Figure 4 presents the carbon and fluorine distributions for a thin and a thick electrode respectively, with no clear distinctions between the samples. The results are in contrast with the findings of Saraka et al. [27] who showed differences in carbon dispersion in NMC electrodes by temperature and shear rate. The data, however, was obtained at a laboratory scale, using a different drying set-up (room temperature, oven or hot plate depending on drying temperature) to the convective drying employed in the present study, a different formulation and a different mixing protocol. All these parameters could have had an impact on the slurry microstructure.

Nevertheless, the results of Saraka et al. [27] show, that at fast-drying conditions, the slurry microstructure during coating and drying mainly depends on the starting slurry microstructure. Similarly, other studies have shown that structural changes during drying are not necessarily due to drying conditions only (temperature and air speed), but that also

depend on the slurry formulation [5]. The statistical analysis of the carbon and fluorine distributions obtained in this work reveal, therefore, that for the considered design space (as dictated by the process variable ranges) the fast-drying conditions are not affecting the microstructure, leaving the slurry formulation as the only determinant of such characteristics. Temperature, however, could be an important variable for other physical properties, for instance, adhesion, as shown for graphite anode formulations [5, 26, 57].

The effect of the operating variables on the output variables is examined quantitatively by the linear models obtained from ANOVA. Table 2 contains the coded coefficients for the models of the form given by Eq. (1) for the responses that showed statistically significant terms (p-value <0.1). The coefficients are considering +1 and -1 as the coded high and low levels of the settings. The coded variables can be converted to actual values by the relationship given by Eq. S1. An example of the graphical representation of the effect of input settings on output variables is shown in Figure 5 for mass loading dry. The models can be used to make predictions of the output variables as a function of the settings of the operating variables as shown in section 3.3. Alternatively, the equations can be used to determine the settings of the operating variables for a desired value of the response.

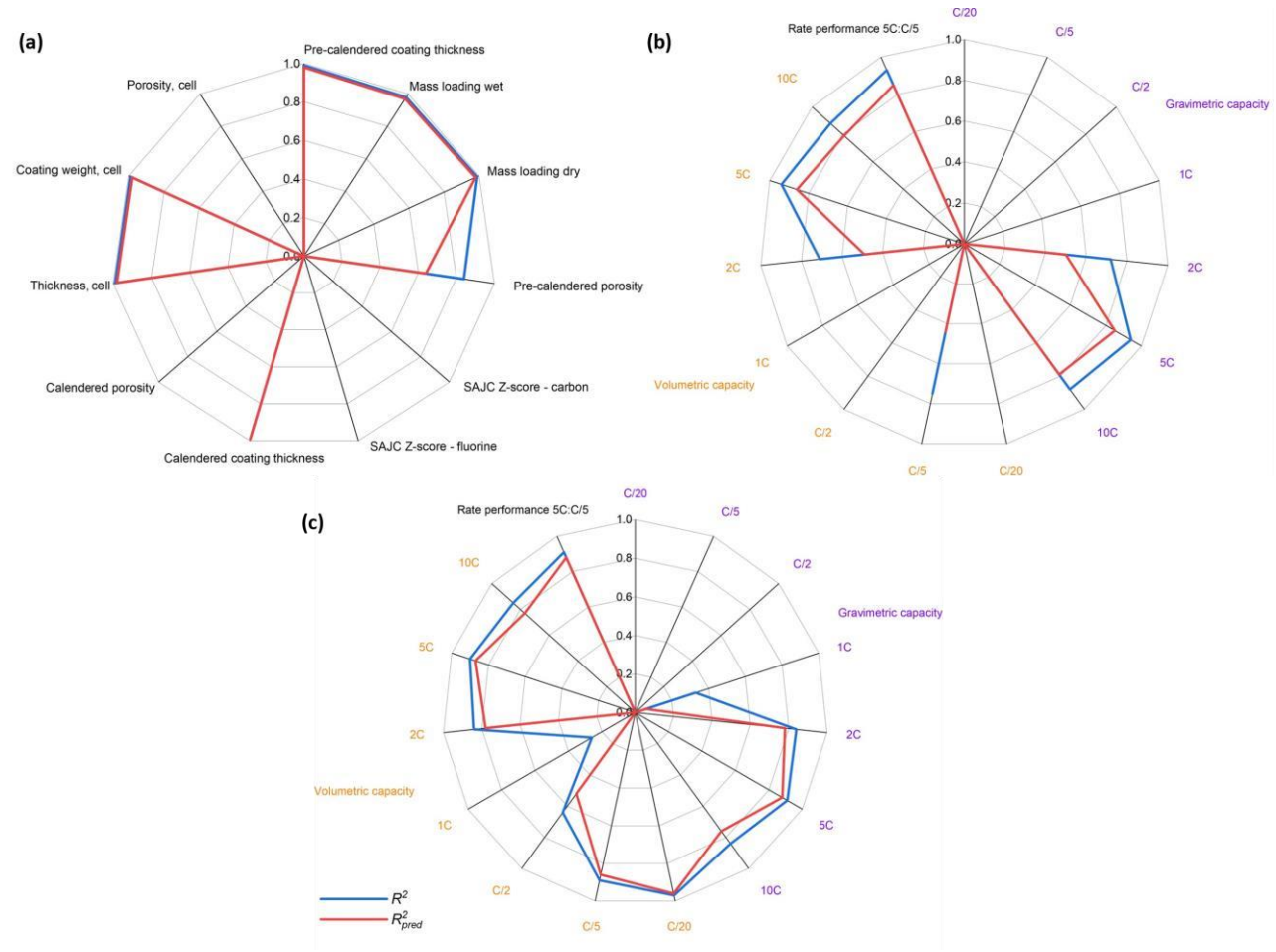

Figure 3. R^2 (blue) and $R_{pred}{}^2$ (red) values for: (a) operating variables – physical properties correlations, (b) operating variables – electrochemical properties correlations and (c) cell physical properties – electrochemical properties correlations.

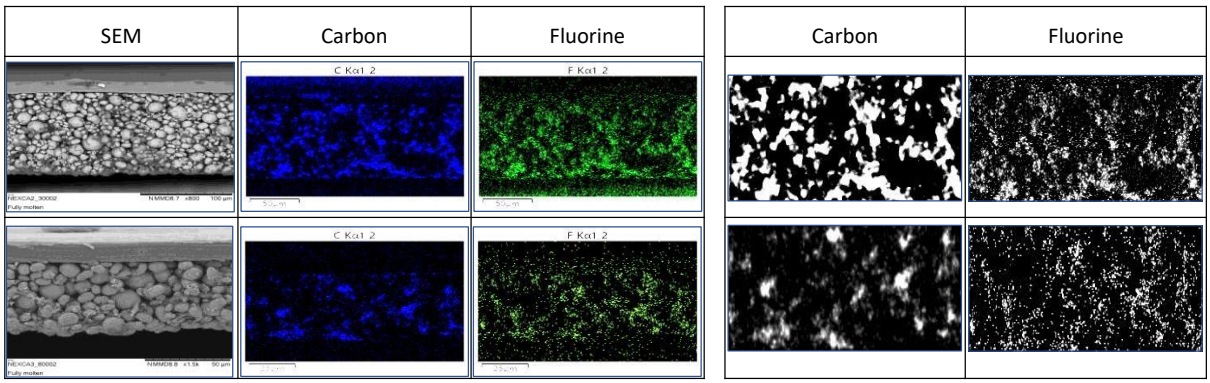

Figure 4. SEM and EDS images (left) and their corresponding black and white conversions (right) showing the carbon and fluorine distributions for: (a) a thick electrode dried at 85 °C (experiment 1 in Table 1), and (b) a thin electrode dried at 110 °C (experiment 6).

Table 2. Transformation parameter (λ) and coded model coefficients (β_i) for the significant terms of the operating variables as factors (x_1 = Comma bar gap, x_2 = Web speed, x_3 = Temperature, x_4 = Air speed and x_5 = Coating ratio).

	Response	□	□$_0$	□$_1$	□$_2$	□$_3$	□$_4$	□$_5$	R^2
Physical properties	Pre-calendered coating thickness	0	1.872	0.0868				0.0569	0.99
	Mass loading wet	-0.5	0.0626	-0.0073				-0.0040	0.98
	Mass loading dry	-0.5 1	0.0759	-0.0086 -				-0.0048	0.99
	Pre-calendered porosity	-0.5	47.80	1.400	-1.128			0.7650	0.84
	Calendered coating thickness	-0.5	0.1339	-0.0154				-0.0082	0.99
	Thickness, cell		0.1329	-0.0159				-0.0075	0.99
	Coating weight, cell	-0.5	0.0761	-0.0091				-0.0048	0.99
Electrochemical properties	Gravimetric capacity at 2C	1	104.80	-27.61				-20.00	0.72
	Gravimetric capacity at 5C	1	52.94	-34.71			-8.76	-16.68	0.94
	Gravimetric capacity at 10C	0	0.981	-0.252				-0.174	0.88
	Volumetric capacity at C/5	1	463.40		-8.85		-7.05	8.39	0.75
	Volumetric capacity at 2C	1	306.34	-82.04				-54.65	0.71
	Volumetric capacity at 5C	1	154.57	-101.29			-25.30	-47.55	0.94
	Volumetric capacity at 10C	0	1.449	-0.252				-0.168	0.88
	Rate performance 5C:C/5	1	33.53	-22.11			-5.31	-10.74	0.93

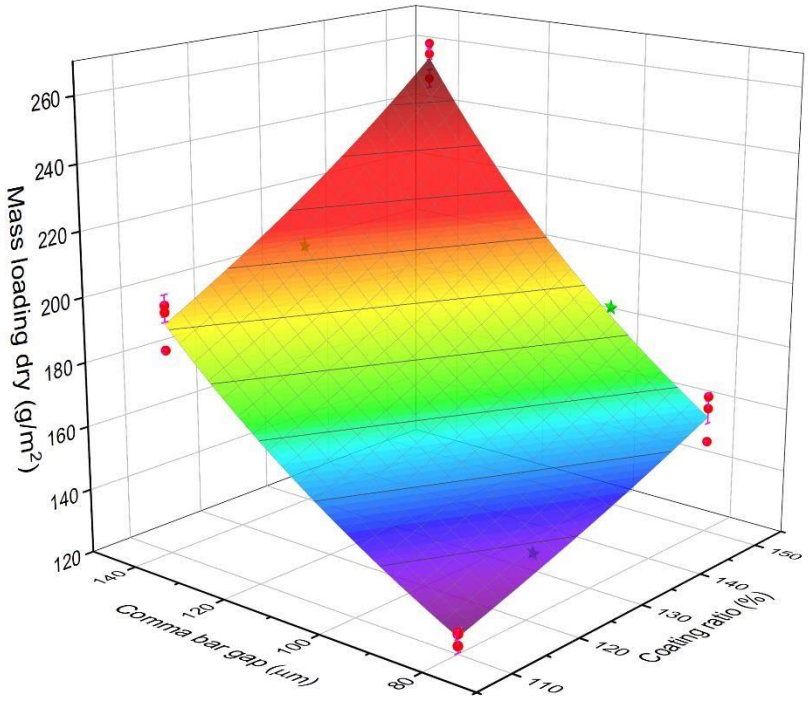

Figure 5. Response surface for the pre-calendered mass loading dry as a function of the main factors: comma bar gap and coating ratio. Dots are experimental data points from the design matrix. Stars are validation experimental points (see section 3.3).

3.1.2 Effect on electrochemical properties

The main influencing factors for most of the gravimetric and volumetric discharge capacities, were comma bar gap and coating ratio (Figure S5). R^2 and $R_{pred}{}^2$ values as high as 0.94 and 0.86, respectively, were obtained in some cases (e.g. 5C gravimetric discharge capacity, Figure 3b). Web speed was also identified as a significant term for volumetric capacity at C/5; however, the $R_{pred}{}^2$ was only of 0.44 making the model unsuitable for predictions. Although web speed only showed statistical significance for two of the total number of responses (precalendered porosity and C/5 volumetric capacity, it should not be completely discarded as

a main factor before a follow-up experimental plan to truly identify its effect on the studied output variables.

For some capacities air speed was also identified as a significant factor (Figure S5), but its contribution to the response was lower than the effects given by the comma bar gap and coating ratio as shown by the coded coefficients (Table 2). Some of the capacities, on the other hand, did not show a correlation with any of the operating variables, specially at C-rates of 1C and below. Although there is no obvious trend between the values of the correlation coefficients and the different C-rates, it seems that a correlation appears at 2C, reaches a maximum at 5C and then decreases at 10C (Figure 3b).

In contrast to drying studies done at a laboratory scale [27, 58], the discharge capacities obtained in this work are independent of drying temperature, at least in the 85 °C – 110 °C range and the design space given by the rest of the settings. As an example, Figure 6 shows the discharge gravimetric capacities for three different C-rates at the two temperatures studied and for thin and thick electrode coatings. No meaningful variation can be observed for the values at the two temperatures. As discussed in section 3.1.1, at fast drying conditions the initial slurry microstructure has a more important effect than the drying conditions.

Rate performance, an important parameter for high power and fast charging applications [59], was correlated mainly to comma bar gap and coating ratio, with some minor effect given by air speed.

The coded coefficients for the statistically significant terms (p-value < 0.1) in the models given by Eq. (1) for all the electrochemical tests are presented in Table 2. Nevertheless, the identified

correlations do not determine causation. As observed by Hawley and Li [18], it is difficult to attribute discrepancies in output only from the variation of the studied parameters since electrode manufacturing is an interconnected process. However, the effects of the two main identified factors, comma bar gap and coating ratio, permeate through the different stages of the manufacturing process and are closely linked to battery performance.

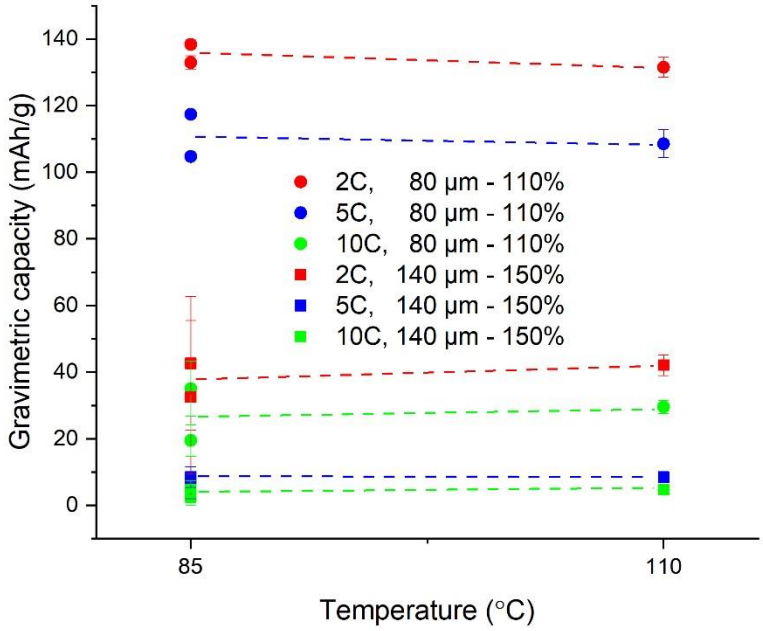

Figure 6. Gravimetric capacities at three different C-rates and two temperatures for coating at 80 µm comma bar gap and 110% coating ratio, and 140 µm comma bar gap and 150% coating ratio. Figures are experimental points from experiments 1, 5, 6 , 7, 9 and 11 in Table 1.

3.2 Regression analysis on half-coin cells

Linear regression analysis was employed to determine the possible relationship between the electrochemical properties of the produced half-coin cells and their physical characteristics (thickness, coating weight and porosity). The models considered in the linear regression were also of the form given by Eq. (1). A higher order polynomial model could have resulted in a better R^2 but at the expense of a lower R^2_{pred}. Additionally, since the analysis of the data was carried out on the obtained data for the screening DoE, and not through a dedicated experimental design (in which the physical properties are the factors and their values determined based on a specific design), there is a risk of multicollinearity of the regression coefficients for higher order polynomials due to the lack of orthogonality, which would have

made the predictions very sensitive to the coefficients used. The final models for the responses were obtained by forward selection of terms based on p-values (< 0.1).

Because thickness varied freely depending on the amount of coating weight, these two properties were strongly correlated (Figure S7), and it was possible to undertake the analysis based on only one of them. The statistical analysis was thus performed using coating weight and the porosity as the only input variables. Slightly different results would have been obtained if thickness had been used instead. Figure S6 and Table 3 show the main physical properties influencing each of the electrochemical measurements according to ANOVA as well as the coded coefficients for the models given by Eq. (1), respectively.

No relationship was found for the C/20, C/5 and C/2 gravimetric capacities with any of the cell physical properties. The 1C and higher gravimetric capacities, on the other hand, showed correlations with coating weight resulting in R^2 up to 0.91 for 5C (Figure 3c). Better performance was observed for the lower coating weights (or lower thicknesses) as shown in Figure 7a.

Porosity was the only important factor for the volumetric capacities at C/20, C/5 and C/2, with better correlations towards the lower C-rates (Figure 3c and Figure S6). Lower porosities resulted in higher volumetric capacities (Figure 7b) as expected from low carbon formulations [27], demonstrating an ionic transport dominated region. The lack of correlation with coating weight for the low C-rate volumetric capacities explains the already observed lack of a relationship between the C/20 and C/2 rates and comma bar gap and coating ratio, since these operating parameters are the only ones responsible for the amount of coating. For the case of

the C/5 rate, porosity is deemed to be a better predictor than the identified main operating parameters for this particular rate (web speed, air speed and coating ratio) as shown by the higher $R_{pr^2\,ed}$ (Figure 3c).

A transition seems to exist at 1C, wherein coating weight overtakes porosity as the dominant physical property. The strength of the correlations tends to increase as the C-rate increases (Figure 3c). However, the poor predictive capabilities of the model at 1C in terms of the physical properties as indicated by the R^2 and R_{pred^2} (Figure 3c), and the absence of correlation with any of the operating variables imply that other factors not considered in the study are the true predictors (e.g. tortuosity or micro-porosity).

The improved performance at lower coating weights is in contrast of the results presented by Hamed et al. [60] in which thicker electrodes result in lower reductions in discharge by the increase in C-rate. One possible reason for the discrepancies are the differences in the formulation (NMC111 vs NMC622) and the NMC loading. Hamed et al. [60] have shown in fact, that performance strongly depends on the NMC loading. Studies with different NMC materials would thus be needed to fully explain such discrepancies but are beyond the scope of the present study. On the other hand, the present results are in line with the findings from Schmidt et al. [15] who showed that the mass loading (by means of the coating step) has the highest impact on volumetric energy density, and that porosity becomes also more or less important depending on C-rate.

In order to analyse the discharge capacity loss across the different C-rates and determine the responsible physical property, a rate capacity coefficient (κ) was calculated from the plot of

$Ln(discharge\ capacity)$ vs $C\text{-}rate$ for each of the experiments (see Figure S8 for an example subset of the results). The gradient of the line corresponds to κ and is the magnitude of the change in capacity by every unit change in C-rate. Higher values of κ mean higher reductions in the discharge capacity. $R^2 \geq 0.9$ for the fitted lines were obtained in all cases. The calculated κ values can be found in the Data in brief publication [50] and are plotted in Figure 7c for reference. The analysis was performed using the gravimetric capacities, but similar results would have been obtained for the volumetric capacities.

The ANOVA on κ reveals that when looking across the different C-rates, the cell coating weight is statistically significant (p-value < 0.0001), with a high degree of correlation and prediction ($R^2 > 0.88$ and $R^2_{pred} > 0.82$). This is consistent with the analysis on individual C-rates that already showed a strong correlation with coating weight for the 1C and higher rates. For the lower C-rates, porosity is the dominant property but when considering the whole range, coating weight is the main parameter. The model coefficients for κ as a function of coating weight are presented in Table 3. Similar to the results on individual C-rates, the electrodes with lower coating weights exhibit improved performance, i.e. result in lower magnitudes of κ (Figure 7c). In line with these results, an analysis of κ as a function of the process parameters reveals a strong correlation with comma bar gap and coating ratio (R^2 and $R^2_{pred} > 0.82$).

Rate performance was explained by coating weight only (R^2 = 0.84), in agreement with the results showing a strong correlation (R^2 = 0.93) with comma bar gap and coating ratio. As expected from the statistical analysis on the individual C-rates and κ, and also as reported in

other studies [59], lower coating weights (or thinner electrodes) performed better (Figure 7d) due to improved electronic and ion transport.

Table 3. Transformation parameter (λ) and coded model coefficients (β_i) for the significant terms of the cell physical properties as factors (x_1 = Coating weight, x_2 = Porosity).

Response	□	□$_0$	□$_1$	□$_2$	R^2
Gravimetric capacity at 1C	1	133.18	-13.11		0.33
Gravimetric capacity at 2C	1	98.87	-51.86		0.84
Gravimetric capacity at 5C	0	1.44	-0.64		0.91
Gravimetric capacity at 10C	0	0.933	-0.422		0.84
Volumetric capacity at C/20	1	475.26		-26.31	0.97
Volumetric capacity at C/5	1	460.32		-24.48	0.89
Volumetric capacity at C/2	1	436.02		-22.25	0.64
Volumetric capacity at 1C	1	390.93	-34.46		0.26
Volumetric capacity at 2C	1	289.15	-150.31		0.84
Volumetric capacity at 5C	0	1.91	-0.64		0.90
Volumetric capacity at 10C	0	1.40	-0.42		0.85
Rate capacity coefficient, κ	1	-0.0249	0.00174		0.88
Rate performance 5C:C/5	0	1.24	-0.64		0.91

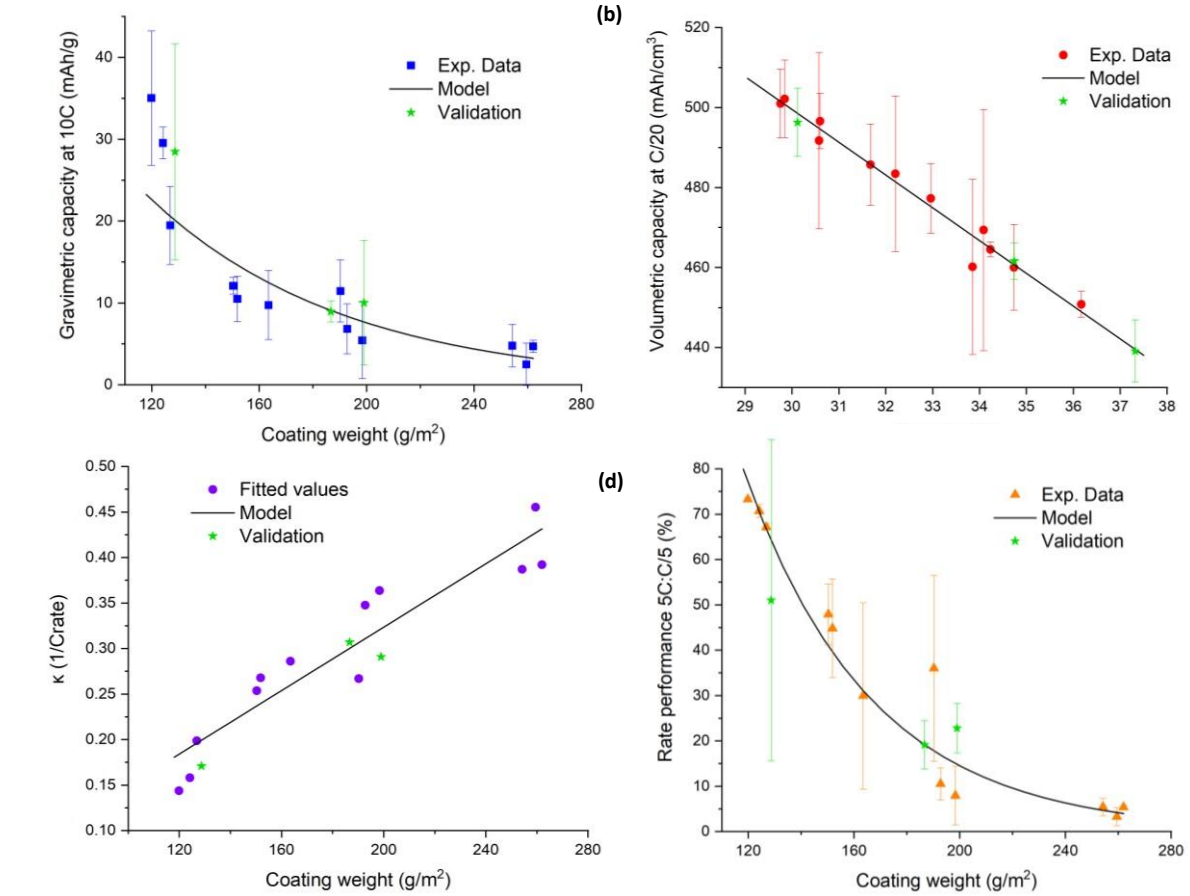
(a)
Gravimetric capacity at 10C (mAh/g)
Exp. Data
Model
Validation
Coating weight (g/m²)
(b)
Volumetric capacity at C/20 (mAh/cm³)
Exp. Data
Model
Validation
(c)
κ (1/Crate)
Fitted values
Model
Validation
Coating weight (g/m²)
(d)
Rate performance 5C:C/5 (%)
Exp. Data
Model
Validation
Coating weight (g/m²)

Figure 7. Performance vs cell physical properties for selected electrochemical properties: (a) gravimetric capacity at 5C, (b) volumetric capacity at C/20, (c) rate capacity coefficient and (d) rate performance at 5C:C/5. Stars are validation experimental points (see section 3.3).

3.3 Model Validation

Three extra experiments were undertaken for model validation at the operating conditions stated in Table 4. The values of the responses for the extra experiments can be found in the Data in Brief publication [50]. The coating weight and porosity of the produced cells are also shown in Table 4 since these are also input variables for the models where the physical properties are the input variables. The experimental values of the responses (y_{exp}) of the $n = 3$ obervations was compared against the predicted values (y_{pred}) from the equations obtained in sections 3.1 and 3.2 by computing the mean relative error (MRE) according to Eq. (5). The computed MREs (Figure 8) demonstrate that the operating variables are good predictors of the electrode and cell physical properties (average MRE=6%), but the electrochemical properties are better predicted using the cell physical characteristics

(average MRE=14%) compared with the case of the operating variables as the inputs (MRE=31%). The relatively low MREs for most cases demonstrate the suitability of the empirical models for prediction purposes. The results of the validation experiments are also plotted in Figure 5 andFigure 7 in order to visualise their deviation from the model output.

Table 4. Operating conditions of the model validation experiments and coating weight and porosity values of the produced cells.

Experiment	Comma bar gap (□m)	Web speed (m/min)	Temperature (°C)	Air speed (m/s)	Coating ratio (%)	Cell coating weight (g/m^2)	Cell porosity (%)
Validation 1	100	1.2	85	5	150	186.7	30.12
Validation 2	85	1	85	15	125	128.7	37.32
Validation 3	120	0.5	85	15	150	199.0	34.74

$$MRE = \frac{100}{n}\sum_{i=1}^{n}\left|\frac{y_{exp,i} - y_{pred,i}}{y_{exp,i}}\right| \quad (5)$$

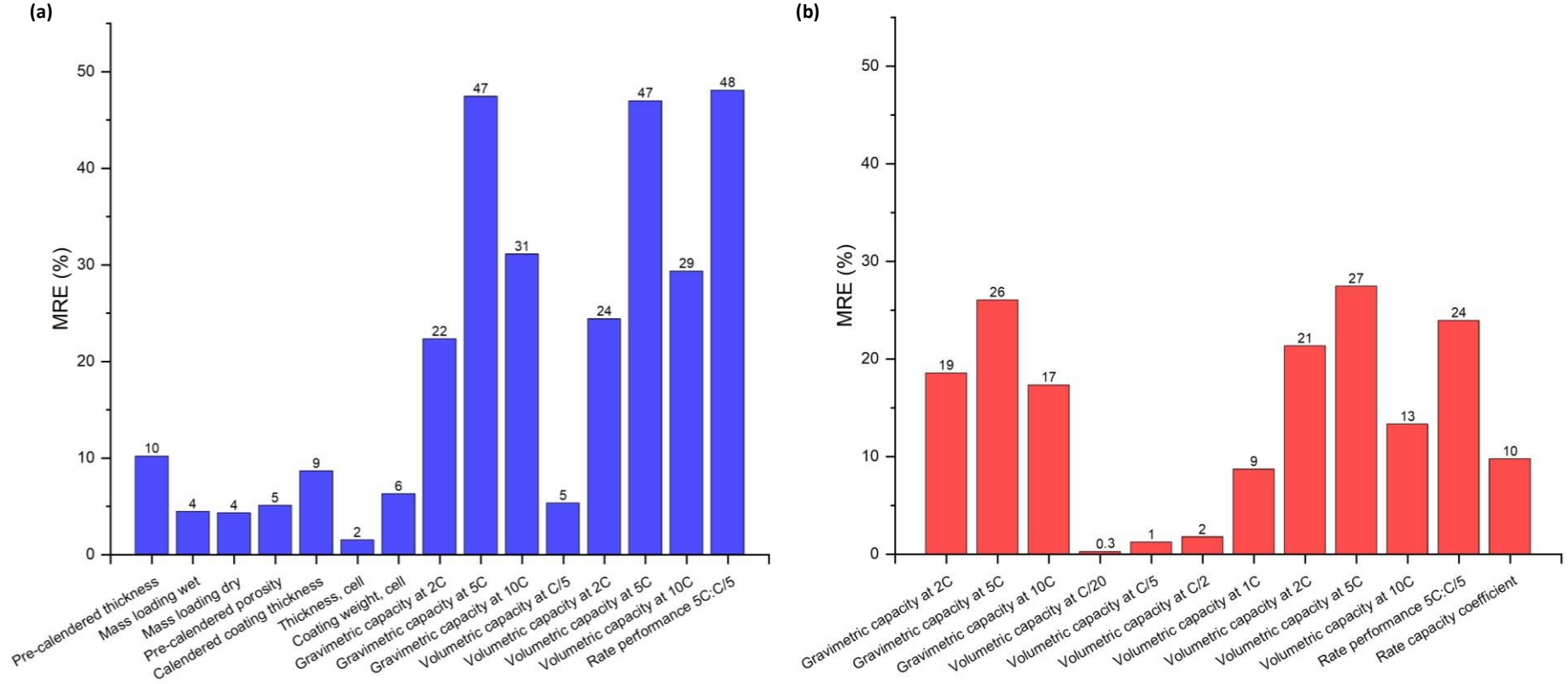

Figure 8. Mean relative error (MRE) for the validation runs: (a) operating variables as factors, (b) cell physical properties as factors.

4 Conclusions

The electrochemical performance of NMC cathodes was studied as a function of process variables (comma bar gap, web speed, drying temperature, air speed and coating ratio) and electrode physical properties (thickness, coating weight and porosity) through statistical analysis at the pilot plant level. Comma bar gap and coating ratio were identified as the main operating parameters influencing the gravimetric and volumetric capacities at different Crates and rate performance. Contrary to studies at laboratory scale, the results show that temperature is not an important process state variable, at least for the constrained operating region given by experimental design. The results are supported by spatial autocorrelation and join counting Z-score which showed no differences in carbon and fluorine distributions. Drying air speed was also identified as a non-significant factor. The settings of the non-important factors can thus be set to their lowest value to reduce operating costs.

Coating weight was identified as the most important property explaining most of the variations of the electrochemical characterisations with thinner electrodes resulting in superior performance. Porosity became an important property only for the volumetric capacities at the lower C-rates. The performance of the battery at the conditions studied mainly depend on the formulation and the mixing protocol and not the drying conditions. The effects of formulation and distribution are simply being transmitted to the final cell by the amount of slurry being coated. From a quality by design perspective, comma bar gap and coating ratio should be considered critical parameters since their settings have a direct impact on battery performance. Based on the results presented, coating weight is therefore deemed to be a critical property.

Further studies varying the formulation and mixing protocol are required to devise whether for a different experimental region, temperature and air speed would still be classified as nonsignificant parameters. Similarly, a follow-up experimental plan would be necessary to assess in more detail the effect of web speed on battery electrochemical performance as well as the effect of factor interactions.

Empirical models representing the relationship between the operating variables, electrode and cell physical characteristics, and the cell electrochemical performance, were obtained by linear regression. Model validation showed the suitability of the models to establish the operating parameters settings required to produce electrodes and cells with specific thicknesses, mass loadings and coating weights, as well as to determine the required coating weights and porosities to achieve targeted gravimetric and volumetric capacities.

Acknowledgments

This research was undertaken through the NEXTRODE project, funded by the Faraday Institution (Grant number: FIRG015).

References

[1] Woodward M, Hamilton J, Walton B, Ringrow J, Alberts G, Fullerton-Smith S, Day E. Electric vehicles. Setting a course for 2030. UK: Deloitte; 2020.

[2] UK Government. The ten point plan for a green industrial revolution. UK 2020.

[3] Armand M, Axmann P, Bresser D, Copley M, Edström K, Ekberg C, Guyomard D, Lestriez B, Novák P, Petranikova M, Porcher W, Trabesinger S, Wohlfahrt-Mehrens M, Zhang H. Lithium-ion batteries – current state of the art and anticipated developments. J Power Sources 2020;479.

[4] Wood DL, Wood M, Li J, Du Z, Ruther RE, Hays KA, Muralidharan N, Geng L, Mao C, Belharouak I. Perspectives on the relationship between materials chemistry and roll-to-roll electrode manufacturing for high-energy lithium-ion batteries. Energy Storage Materials 2020;29:254-65.

[5] Westphal B, Bockholt H, Gunther T, Haselrieder W, Kwade A. Influence of convective drying parameters on electrode performance and physical electrode properties. ECS Transactions 2015;64:57-68.

[6] Hasa I, Mariyappan S, Saurel D, Adelhelm P, Koposov AY, Masquelier C, Croguennec L, CasasCabanas M. Challenges of today for Na-based batteries of the future: From materials to cell metrics. J Power Sources 2021;482:228872.

[7] Salini PS, Gopinadh SV, Kalpakasseri A, John B, Thelakkattu Devassy M. Toward greener and sustainable Li-ion cells: An overview of aqueous-based binder systems. ACS Sustainable Chem Eng 2020;8:4003-25.

[8] Rynne O, Dubarry M, Molson C, Nicolas E, Lepage D, Prébé A, Aymé-Perrot D, Rochefort D, Dollé M. Exploiting materials to their full potential, a li-ion battery electrode formulation optimization study. ACS Appl Energy Mater 2020;3:2935-48.

[9] Rojaee R, Shahbazian-Yassar R. Two-dimensional materials to address the lithium battery challenges. ACS Nano 2020;14:2628-58.

[10] Manthiram A. A reflection on lithium-ion battery cathode chemistry. Nat Commun 2020;11:1550.

[11] Heck CA, von Horstig M-W, Huttner F, Mayer JK, Haselrieder W, Kwade A. Review—knowledgebased process design for high quality production of NCM811 cathodes. J Electrochem Soc 2020;167:160521.

[12] Ji X, Xia Q, Xu Y, Feng H, Wang P, Tan Q. A review on progress of lithium-rich manganese-based cathodes for lithium ion batteries. J Power Sources 2021;487:229362.

[13] Gallagher KG, Trask SE, Bauer C, Woehrle T, Lux SF, Tschech M, Lamp P, Polzin BJ, Ha S, Long B, Wu Q, Lu W, Dees DW, Jansen AN. Optimizing areal capacities through understanding the limitations of lithium-ion electrodes. J Electrochem Soc 2015;163:A138-A49.

[14] Kwade A, Haselrieder W, Leithoff R, Modlinger A, Dietrich F, Droeder K. Current status and challenges for automotive battery production technologies. Nat Energy 2018;3:290-300.

[15] Schmidt O, Thomitzek M, Röder F, Thiede S, Herrmann C, Krewer U. Modeling the impact of manufacturing uncertainties on lithium-ion batteries. J Electrochem Soc 2020;167:060501.

[16] Mohanty D, Hockaday E, Li J, Hensley DK, Daniel C, Wood DL. Effect of electrode manufacturing defects on electrochemical performance of lithium-ion batteries: Cognizance of the battery failure sources. J Power Sources 2016;312:70-9.

[17] Westermeier M, Reinhart G, Zeilinger T. Method for quality parameter identification and classification in battery cell production quality planning of complex production chains for battery cells. 3rd International Electric Drives Production Conference (EDPC) 2013. p. 1-10.

[18] Hawley WB, Li J. Electrode manufacturing for lithium-ion batteries—analysis of current and next generation processing. J Energy Storage 2019;25:100862.

[19] Turetskyy A, Thiede S, Thomitzek M, von Drachenfels N, Pape T, Herrmann C. Toward data-driven applications in lithium-ion battery cell manufacturing. Energy Technol 2020;8:1900136-.

[20] Meyer O, Weihs C, Mähr S, Tran H-Y, Kirchhof M, Schnackenberg S, Neuhaus-Stern J, Rößler S, Braunwarth W. Development and implementation of statistical methods for quality optimization in the large-format lithium-ion cells production. Energy Technol 2020;8:1900244.

[21] Schnell J, Nentwich C, Endres F, Kollenda A, Distel F, Knoche T, Reinhart G. Data mining in lithiumion battery cell production. J Power Sources 2019;413:360-6.

[22] Westermeier M, Reinhart G, Steber M. Complexity management for the start-up in lithium-ion cell production. Procedia CIRP. C ed2014. p. 13-9.

[23] Bockholt H, Indrikova M, Netz A, Golks F, Kwade A. The interaction of consecutive process steps in the manufacturing of lithium-ion battery electrodes with regard to structural and electrochemical properties. J Power Sources 2016;325:140-51.

[24] Lenze G, Bockholt H, Schilcher C, Froböse L, Jansen D, Krewer U, Kwade A. Impacts of variations in manufacturing parameters on performance of lithium-ion-batteries. J Electrochem Soc 2018;165:A314-A22.

[25] Müller M, Pfaffmann L, Jaiser S, Baunach M, Trouillet V, Scheiba F, Scharfer P, Schabel W, Bauer W. Investigation of binder distribution in graphite anodes for lithium-ion batteries. J Power Sources 2017;340:1-5.

[26] Jaiser S, Müller M, Baunach M, Bauer W, Scharfer P, Schabel W. Investigation of film solidification and binder migration during drying of li-ion battery anodes. J Power Sources 2016;318:210-9.

[27] Saraka RM, Morelly SL, Tang MH, Alvarez NJ. Correlating processing conditions to short- and longrange order in coating and drying lithium-ion batteries. ACS Appl Energy Mater 2020;3:11681-9.

[28] Terashita K, Asano H, Miyanami K. Kneading and dispersing of electrode materials for secondary lithium ion batteries. KONA Powder and Particle Journal 2001;19:254-61.

[29] Wang M, Dang D, Meyer A, Arsenault R, Cheng Y-T. Effects of the mixing sequence on making lithium ion battery electrodes. J Electrochem Soc 2020;167:100518.

[30] Westphal BG, Mainusch N, Meyer C, Haselrieder W, Indrikova M, Titscher P, Bockholt H, Viöl W, Kwade A. Influence of high intensive dry mixing and calendering on relative electrode resistivity determined via an advanced two point approach. J Energy Storage 2017;11:76-85.

[31] Hoffmann L, Grathwol JK, Haselrieder W, Leithoff R, Jansen T, Dilger K, Dröder K, Kwade A, Kurrat M. Capacity distribution of large lithium-ion battery pouch cells in context with pilot production processes. Energy Technol 2020;8.

[32] Bockholt H, Haselrieder W, Kwade A. Intensive powder mixing for dry dispersing of carbon black and its relevance for lithium-ion battery cathodes. Powder Technol 2016;297:266-74.

[33] Westphal BG, Kwade A. Critical electrode properties and drying conditions causing component segregation in graphitic anodes for lithium-ion batteries. J Energy Storage 2018;18:509-17.

[34] Yourey W. Theoretical impact of manufacturing tolerance on lithium-ion electrode and cell physical properties. Batteries 2020;6:23.

[35] Schönemann M, Bockholt H, Thiede S, Kwade A, Herrmann C. Multiscale simulation approach for production systems: Application to the production of lithium-ion battery cells. Int J Adv Manuf Technol 2019;102:1373-90.

[36] Thomitzek M, Schmidt O, Röder F, Krewer U, Herrmann C, Thiede S. Simulating process-product interdependencies in battery production systems. Procedia CIRP 2018. p. 346-51.

[37] Laue V, Schmidt O, Dreger H, Xie X, Röder F, Schenkendorf R, Kwade A, Krewer U. Model-based uncertainty quantification for the product properties of lithium-ion batteries. Energy Technol 2020;8:1900201.

[38] Faraji-Niri M, Liu K, Apachitei G, Román-Ramírez LA, Widanage D, Marco J. Data mining for quality prediction of battery in manufacturing process: Cathode coating process. 12th International Conference on Applied Energy (ICAE 2020). Thailand/Virtual 2020. p. 1-5.

[39] Montgomery DC. Design and analysis of experiments. 9th ed. USA: Wiley; 2017.

[40] Mäkelä M. Experimental design and response surface methodology in energy applications: A tutorial review. Energy Convers Manage 2017;151:630-40.

[41] Bowden GD, Pichler BJ, Maurer A. A design of experiments (DoE) approach accelerates the optimization of copper-mediated ^{18}F-fluorination reactions of arylstannanes. Sci Rep 2019;9:11370. [42] Weissman SA, Anderson NG. Design of experiments (DoE) and process optimization. A review of recent publications. Org Process Res Dev 2015;19:1605-33.

[43] N. Politis S, Colombo P, Colombo G, M. Rekkas D. Design of experiments (DoE) in pharmaceutical development. Drug Dev Ind Pharm 2017;43:889-901.

[44] Schnell J, Reinhart G. Quality management for battery production: A quality gate concept. Procedia CIRP 2016. p. 568-73.

[45] NIST/SEMATECH. 5. Process improvement. e-Handbook of Statistical Methods. USA: NIST; 2012. https://www.itl.nist.gov/div898/handbook/pri/pri.htm [accessed 5 May 2020].

[46] Plackett RL, Burman JP. The design of optimum multifactorial experiments. Biometrika 1946;33:305-25.

[47] Cunha RP, Lombardo T, Primo EN, Franco AA. Artificial intelligence investigation of NMC cathode manufacturing parameters interdependencies. Batteries Supercaps 2020;3:60-7.

[48] Stat-Ease Inc. Design-expert® software, version 13. Minneapolis, MN, USA2020.

[49] Rynne O, Dubarry M, Molson C, Lepage D, Prébé A, Aymé-Perrot D, Rochefort D, Dollé M. Designs of experiments for beginners—a quick start guide for application to electrode formulation. Batteries 2019;5:72.

[50] Román-Ramírez LA, Apachitei G, Faraji Niri M, Lain M, Widanage D, Marco J. Experimental data of cathodes manufactured in a convective dryer at the pilot-plant scale, and charge and discharge capacities of half-coin lithium-ion cells. 2021;Submitted.

[51] MATLAB. Version 2020a.: The MathWorks Inc.; 2020.

[52] Moran PAP. Notes on continuous stochastic phenomena. Biometrika 1950;37:17-23.

[53] Geary RC. The contiguity ratio and statistical mapping. The Incorporated Statistician 1954;5:11546.

[54] Cliff AD, Ord K. Spatial autocorrelation: A review of existing and new measures with applications. Econ Geogr 1970;46:269-92.

[55] Schneider CA, Rasband WS, Eliceiri KW. NIH image to ImageJ: 25 years of image analysis. Nat Methods 2012;9:671-5.

[56] Primo EN, Chouchane M, Touzin M, Vazquez P, Franco AA. Understanding the calendering processability of $Li(Ni_{0.33}Mn_{0.33}Co_{0.33})O_2$-based cathodes. J Power Sources 2021;488: 229361.

[57] Baunach M, Jaiser S, Schmelzle S, Nirschl H, Scharfer P, Schabel W. Delamination behavior of lithium-ion battery anodes: Influence of drying temperature during electrode processing. Drying Technol 2016;34:462-73.

[58] Stein M, Mistry A, Mukherjee PP. Mechanistic understanding of the role of evaporation in electrode processing. J Electrochem Soc 2017;164:A1616-A27.

[59] Tian R, Park S-H, King PJ, Cunningham G, Coelho J, Nicolosi V, Coleman JN. Quantifying the factors limiting rate performance in battery electrodes. Nat Commun 2019;10:1-11.

[60] Hamed H, Yari S, D'Haen J, Renner FU, Reddy N, Hardy A, Safari M. Demystifying charge transport limitations in the porous electrodes of lithium-ion batteries. Adv Energy Mater 2020;10:2002492.